Scanning capacitance spectroscopy of an $Al_xGa_{1-x}N$/GaN heterostructure field-effect transistor structure: Analysis of probe tip effects

D. M. Schaadt and E. T. Yu[a)]
Department of Electrical and Computer Engineering, University of California at San Diego, La Jolla, California 92093

(Received 7 January 2002; accepted 17 March 2002)

We have performed an analysis of the influence of the probe tip geometry in scanning capacitance microscopy and spectroscopy measurements on an $Al_xGa_{1-x}N$/GaN heterostructure field-effect transistor (HFET) structure. The extremely small probe tip size (typical apex radius ~10–30 nm) makes a detailed analysis essential in comparisons of *dC/dV* spectra with standard, large-area *C/V* measurements. Using three-dimensional simulation software, we have calculated *dC/dV* spectra for various tip geometries and have found that the nanoscale tip structure influences *dC/dV* spectra strongly, while the macroscopic shape has a much smaller influence on the *dC/dV* spectra. Thus, caution must be exercised in comparison of individual *dC/dV* spectra obtained over periods during which the probe tip geometry might have changed. We have analyzed these effects in detail and assessed their influence on the extraction of parameters such as threshold voltage, layer thickness, doping concentrations, and information about trap states in nitride HFETs and other electronic device structures. [DOI: 10.1116/1.1491536]

I. INTRODUCTION

Scanning capacitance microscopy (SCM) in combination with scanning capacitance spectroscopy (SCS) has been used extensively for nanometer- to submicron-scale characterization of electronic structure in semiconductors. Notable applications have included two-dimensional dopant profiling on Si-based device structures[1–3] and imaging of local electronic properties in group III–nitride heterostructure field-effect transistors (HFETs).[4,5] In SCS a bias voltage, consisting of a high frequency ac bias V_{ac} added to a slowly varying dc bias ramp V_{dc}, is applied between the sample and a conductive probe tip, and *dC/dV* versus V_{dc} spectra are recorded as a function probe position. While qualitative interpretation of SCM images and SCS spectra is in many instances well understood, quantitative interpretation of SCM results requires careful analysis of, among other factors, the role of the probe tip.[6,7] Thus far, only limited studies on the detailed effects of the probe tip geometry on the *dC/dV* spectra have been reported. For instance, blunt tips often result from scanning for long periods of time over which the tip shows increasing wear. Based on limited simulation of a round versus a flat tip with a radius of curvature of 35 nm, it has been reported that the SCM signal is affected significantly as the tip changes from round to flat shape.[7] In addition, it has been reported that *dC/dV* spectra cannot be described with a simple parallel plate capacitor model due to the effect of the fringing fields and that two-dimensional electrostatic simulations are required to calculate *dC/dV* spectra for a fixed tip size and shape.[8]

In this article, we describe in detail the SCS technique, discuss the direct comparison of SCS spectra with standard, large-area capacitance–voltage (*C–V*) measurements, and provide a detailed analysis of the effects of the probe tip geometry and an assessment of their influence on the extraction of parameters such as threshold voltage, doping concentrations, layer thickness, and information about trap states in nitride HFETs and other electronic device structures.

II. SCANNING CAPACITANCE SPECTROSCOPY

SCM is performed in an atomic-force microscope[9] with an ultrahigh frequency resonant capacitance sensor connected to a grounded probe tip via a transmission line, which is attached to an oscillator and sensing circuit and tuned near its resonance frequency of about 900 MHz. When the tip is brought into contact with a sample, a shift in resonance frequency Δf occurs due to the resulting tip–sample capacitive load C on the transmission line,[10] and a sensor output voltage V_{so}, which is given by

$$V_{so} = c\Delta f, \tag{1}$$

where c is a constant, is measured.[11] The tip–sample capacitance C can be probed in the usual manner by modulating carriers in the sample with a sample bias containing ac and dc components, $V_s = V_{dc} + V_{ac}\sin(\omega_{ac}t)$. It is generally assumed that the resonance frequency shift Δf and thus the measured sensor output voltage is proportional to the derivative *dC/dV* of the tip–sample capacitance at a given dc bias V_{dc}. A quadrature lock-in amplifier can then be used to measure the capacitance sensor output with a high signal-to-noise ratio.[10] Two reference signals, $\sin(\omega_{ac}t+\phi)$ and $\cos(\omega_{ac}t+\phi)$ are used, where ϕ is the base offset between

[a)]Electronic mail: ety@ece.ucsd.edu

the reference signals and the bias applied to the sample. In polarity mode,[10] the output voltage of the capacitance sensor is measured with respect to the reference signal $\sin(\omega_{ac}t+\phi)$ and is given by

$$\overline{V_{so}}=\frac{1}{T}\int_0^T V_{so}(t)\cdot\sin(\omega_{ac}t+\phi)dt,\quad T=\frac{2\pi}{\omega_{ac}}. \tag{2}$$

It is thus necessary to optimize the phase offset between the reference signal and the sample bias in this mode of operation to obtain the maximum output voltage. To avoid this problem, it is possible to measure the output voltage with respect to each reference signal and calculate its magnitude as follows:

$$\overline{V_{so}}=\sqrt{\left(\frac{1}{T}\int_0^T V_{so}(t)\cdot\sin(\omega_{ac}t+\phi)dt\right)^2+\left(\frac{1}{T}\int_0^T V_{so}(t)\cdot\cos(\omega_{ac}t+\phi)dt\right)^2}. \tag{3}$$

This mode of operation is referred to as magnitude mode,[10] and the resulting capacitance sensor output voltage is independent of the phase shift between the reference signals and the applied bias.

The modulation of the resonant frequency Δf arising from the ac component of the sample bias voltage $\Delta V_s = V_{ac}\sin(\omega_{ac}t)$ can then be calculated using a first-order Taylor series approximation for V_s near V_{dc}, as follows:

$$\Delta f=f[V_{dc}+V_{ac}\sin(\omega_{ac}t)]-f(V_{dc})\approx\left.\frac{df}{dV}\right|_{V_{dc}}V_{ac}\sin(\omega_{ac}t) \tag{4}$$

with

$$\frac{df}{dV}=\frac{\partial f}{\partial C}\frac{dC}{dV}=\gamma(f,C)\frac{f}{C}\frac{dC}{dV}\approx\gamma_0\frac{f_d}{C}\frac{dC}{dV}, \tag{5}$$

where f_d is the drive frequency and $\gamma(f,C)\approx\gamma_0$ is the frequency sensitivity,[11] which is approximately constant and equal to 0.5 for $f=f_d$ and for small changes in C. For operation in magnitude mode, we finally obtain using Eqs. (1) and (3):

$$\overline{V_{so}}\approx\frac{1}{2}\left|c\,\gamma_0 f_d\frac{1}{C}\left.\frac{dC}{dV}\right|_{V_{dc}}V_{ac}\right|. \tag{6}$$

This analysis confirms that the measured frequency shift and thus the measured change in sensor output voltage is proportional to the derivative dC/dV of the tip–sample capacitance at a given dc bias V_{dc}. This has implications for measurements of C–V curves ranging from depletion to accumulation or inversion, which will be discussed in Sec. III.

III. THEORETICAL MODELING AND COMPARISON WITH EXPERIMENT

A. Parallel-plate capacitor model

As mentioned in Sec. I, dC/dV spectra obtained in SCM cannot be accurately described using a simple parallel-plate capacitor model because of the importance of fringing fields at small tip–sample contact areas.[8] This effect is illustrated in Fig. 1, in which a comparison is shown of a standard large-area C–V measurement with a dC/dV spectrum obtained in SCM, both measured on an $Al_xGa_{1-x}N/GaN$ HFET structure.[4] The large-area C–V curve, shown in Fig. 1(a) as a solid line, was obtained with an ac bias of 250 mV at a frequency of 100 kHz and with an In Schotty contact ~500 μm×500 μm in size. The dC/dV spectrum, shown in Fig. 1(b) as a dashed line, was obtained in a SCM with a CoCr probe tip and an ac bias of 250 mV at a frequency of 100 kHz. To enable direct comparison of these measurements, either an integration of the dC/dV spectrum, indicated by the various dashed or dotted lines in Fig. 1(a), or a differentiation of the large-area C–V curve with respect to V, shown in Fig. 1(b) by the solid line, is necessary. It is apparent from Fig. 1 that curves obtained via integration of the measured dC/dV spectrum are characterized by a much broader transition than that exhibited by the measured large-area C–V curve, and that the peak of the dC/dV spectrum in Fig. 1(b) is broader than that for the differentiated large-area C–V curve. The difference between the large-scale and small-scale mea-

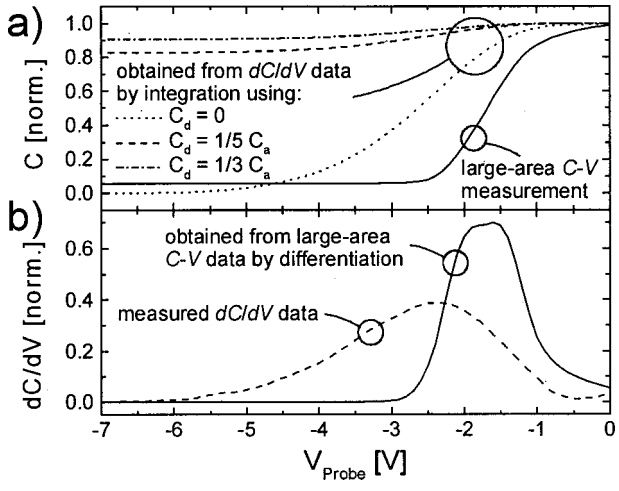

FIG. 1. (a) Plots of a C–V characteristic measured for a large-area Schottky contact and of C–V curves obtained via integration of a local dC/V spectrum, measured by scanning capacitance spectroscopy, for different integration constants. (b) Corresponding dC/dV curves showing the influence of the tip area. The dC/dV curves are normalized to the peak area, i.e., to the accumulation capacitance in (a).

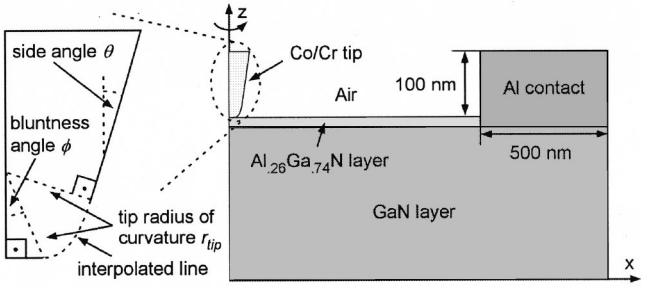

FIG. 2. Schematic diagram of the simulated tip shape and sample structure. The tip is characterized by the radius of curvature r_{tip}, the side angle θ, and the bluntness ϕ, which is given by the angle up to which the tip apex remains flat. The tip–sample contact area is given approximately by $A \approx \pi(r_{tip} \sin \phi)^2$.

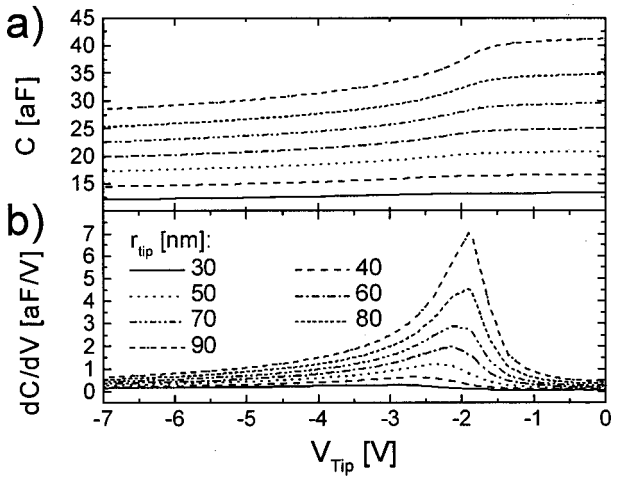

FIG. 3. (a) Simulated $C-V$ curves and (b) corresponding dC/dV spectra for tip radii of curvature ranging from 30 to 90 nm in steps of 10 nm. As the radius of curvature increases, the difference between accumulation and depletion capacitance, and thus the peak height in the dC/dV spectra, increases.

surements is a result of the strong dependence of the depletion depth on the tip–sample contact area, as described in detail in Sec. III B. These results show clearly that it is essential to take the tip size and shape into account, which we have done using numerical simulations of the electrostatic potential. The studies described in Sec. III B extend considerably beyond those previously reported,[6–8,12] which generally do not consider the precise influence of the nanoscale tip shape on the dC/dV spectra.

An additional difficulty arises in the comparison between large-area $C-V$ measurements and local dC/dV spectra. Since the derivatives of the capacitance in depletion and accumulation/inversion are nearly zero, integration of the dC/dV curve will not yield the ratio between depletion and accumulation/inversion capacitance, or the depletion, accumulation, or inversion capacitance itself. The depletion capacitance is given by the integration constant and cannot be obtained directly from the dC/dV data. The effect of this integration constant on the $C-V$ curves obtained by integration is shown in Fig. 1(a) for different assumptions of the ratio between depletion capacitance C_d and accumulation capacitance C_a. As one can see, the shape of the $C-V$ curves depends strongly on the assumed depletion capacitance. It is therefore necessary either to obtain additional information about the depletion or accumulation capacitance in order to fit model $C-V$ curves to integrated experimental dC/dV spectra, or to simulate dC/dV spectra directly for a specific sample structure and tip shape.

B. Numerical simulations

Using commercial three-dimensional device simulation software,[13] we have calculated dC/dV spectra for an $Al_{0.26}Ga_{0.74}N$/GaN HFET epitaxial layer structure, taking into account several possible variations in tip geometry. Spectra were obtained by numerical solutions of Poisson's equation in cylindrical coordinates, with the tip shape defined by the radius of curvature r_{tip}, a characteristic angle of bluntness ϕ defined as the angle up to which the tip remains flat and is in direct contact with the sample, and the side angle θ as shown in a schematic drawing for the simulated structure in Fig. 2. The tip radius of curvature and bluntness angle quantify the nanoscale structure of the tip apex, and the side angle describes the macroscopic structure of probe tips typically employed in SCM. Thus, the simulated tip geometries do not correspond exactly to actual probe tip structures, but are reasonable approximations and allow the simulation of the most influential geometric factors on the dC/dV spectra. The simulated sample structure, which corresponds to an actual sample for which experimental SCS data are shown in Fig. 1, consists of 13 nm $Al_{0.26}Ga_{0.74}N$ doped n type at a concentration of 1×10^{18} cm^{-3} atop a 250 nm GaN layer with a donor concentration of 1×10^{16} cm^{-3}. Fixed polarization charges at the $Al_{0.26}Ga_{0.74}N$/GaN interface and at the $Al_{0.26}Ga_{0.74}N$ surface are simulated by heavily doped 4 and 2 Å thick layers next to the interface and surface, respectively. The dopant concentration in the interface polarization charge layer is chosen such that, if multiplied by the layer thickness of 4 Å, the equivalent of the theoretically predicted polarization charge[14] is obtained. The dopant concentration in the surface polarization charge layer is chosen such that the experimentally measured two-dimensional electron gas electron concentration at zero bias and the threshold voltage for a large-area Ni Schottky contact are approximately reproduced. A work function of 4.9 V is assumed for the tip metal to simulate a Co/Cr tip, which is commonly used in SCM. The tip shape and size are characterized by a tip radius of curvature ranging from 30 to 90 nm, side angles ranging from 15° to 25°, and various degrees of tip bluntness ranging from 5° to 40°. The lower limit of 30 nm for the tip radius of curvature is chosen since it corresponds to an actual apex radius $r_a = r_{tip} \sin\phi$ of ~3–20 nm for the simulated range of bluntness and is thus comparable to sharp probe tips employed in SCM and SCS. The upper limits of $r_{tip} = 90$ nm and $\phi = 40°$ correspond to an actual apex radius of 60 nm and represent a blunt tip. The side ohmic contact is simulated by an Al layer with a work function of 4.1 V, placed on top of the GaN layer as shown in Fig. 2. $C-V$ curves are derived

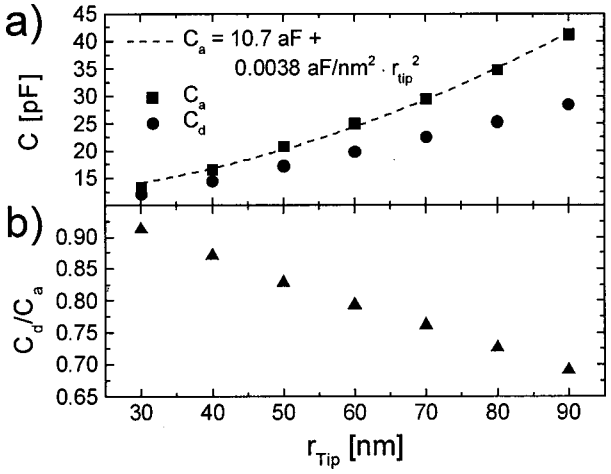

FIG. 4. (a) Plot of the simualted accumulation capacitance C_a at 0 V and the depletion capacitance C_d at -7 V as a function of tip radius of curvature r_{tip}. The dotted line represents a fit to the accumulation capacitance of the form $C_a^{\text{fit}}=a+br_{\text{tip}}^2$. (b) Plot of the depletion capacitance normalized to the accumulation capacitance, indicating that the C_d/C_a decreases with increasing tip radius of curvature.

using an ac tip bias of 250 mV amplitude at a frequency of 100 kHz to simulate typical conditions in SCM measurements. From these C–V curves, dC/dV spectra are calculated by differentiation.

Figure 3 shows simulated C–V curves and the corresponding dC/dV spectra as a function of tip radius of curvature r_{tip} for a side angle of 20° and bluntness angle of 20°. As the tip radius of curvature increases, the difference between the accumulation capacitance and the depletion capacitance increases. This has a very pronounced effect on the dC/dV spectra as seen in Fig. 3(b). The peak height and position are strongly dependent on the tip size. Figure 4 shows plots of the accumulation and depletion capacitances C_a and C_d, respectively, as a function of tip radius of curvature. The dashed line represents a fit to the accumulation capacitance of the form $C_a^{\text{fit}}=a+b\ r_{\text{tip}}^2$, with $a=10.7$ aF and $b=0.0038$ aF/nm^2. It is expected that the accumulation capacitance is proportional to the tip–sample contact area A, which is approximately given by $A\approx\pi(r_{\text{tip}}\sin\phi)^2$ for a tip radius of curvature r_{tip} and an angle of bluntness of ϕ. The accumulation capacitance should therefore be given approximately by $C_a\approx 0.022$ aF/nm^2 r_{tip}^2. This is in good agreement with the form of the fitted curve aside from the constant offset, which is a result of the fringing fields extending from the side of the probe tip. This shows that the accumulation capacitance scales with the tip–sample contact area as expected. On the other hand, the plot of the depletion capacitance normalized to the accumulation capacitance, and thus to the contact area, shows that the normalized depletion capacitance does not scale with contact area and decreases with increasing tip radius of curvature. This is a result of increasing depletion depth with increasing contact area, as shown in Fig. 5. As the tip–sample contact area increases, the depletion radius remains approximately equal to the tip–sample contact area radius; however, the depletion depth increases and thus the

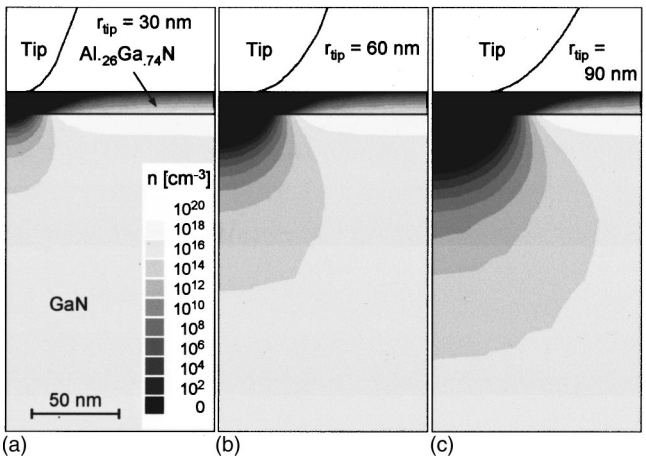

FIG. 5. Plots of the electron concentration in the $Al_{0.26}Ga_{0.74}N$ layer and the GaN layer of a HFET structure at a tip bias of -7 V for tip geometries with a bluntness angle of 20° and a side angle of 20° and radii of curvature of (a) 30 nm, (b) 60 nm, and (c) 90 nm. The dark areas (low electron concentration) correspond to the depletion region. With increasing tip radius of curvature, the depletion radius remains approximately equal to the contact area radius, while the depletion depth increases, causing a decrease in depletion capacitance relative to accumulation capacitance.

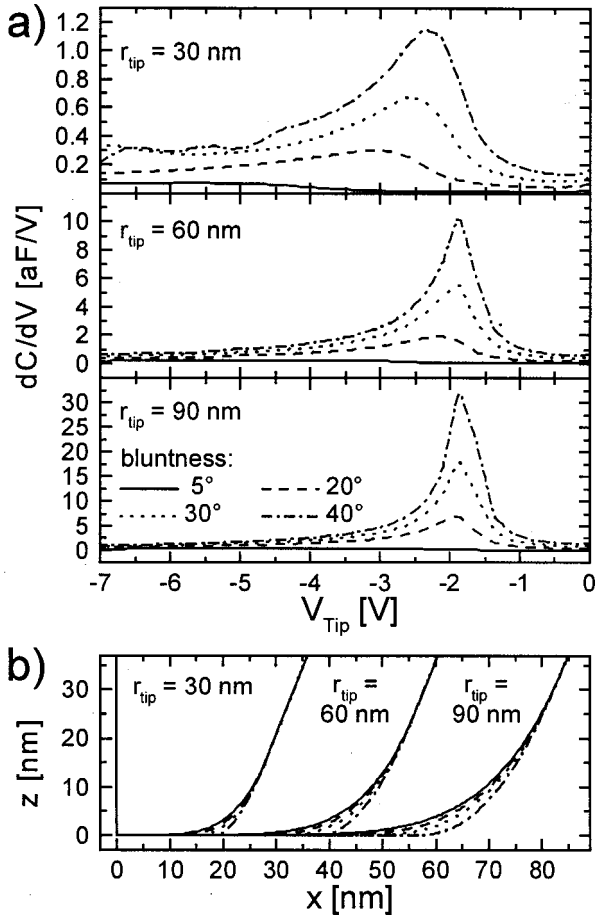

FIG. 6. (a) Plots of simulated dC/dV spectra for tip geometries with a fixed side angle of 20°, tip radii of curvature of 30, 60, and 90 nm, and bluntness angles of 20°, 30°, and 40°. The peak height and position depend strongly on the bluntness angle, with the most prominent effect on the peak position occurring for small tip radii of curvature. (b) Diagrams of the lower portion of the simulated tip geometries.

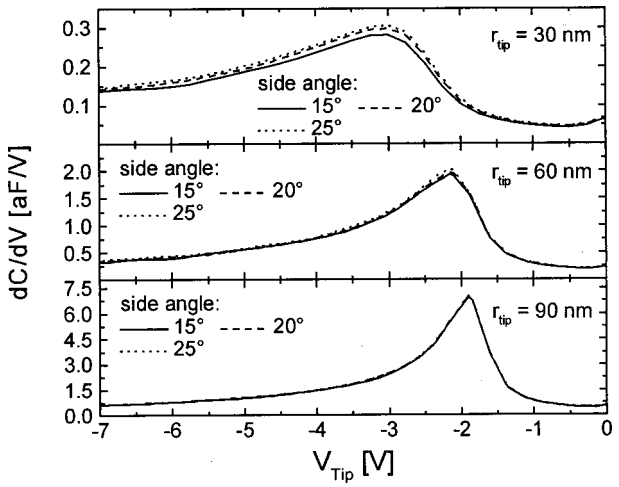

FIG. 7. Simulated *dC/dV* spectra for several tip radii as a function of side angle. The side angle has a negligible effect on the *dC/dV* spectra.

depletion capacitance decreases. This results in a large difference between C_a and C_d, and thus in a large peak height in the *dC/dV* spectra. The increase in peak height allows a higher resolution in the dC/dV signal, but this is offset by a decrease in lateral resolution due to the increase in tip–sample contact area.

To assess the influence of the contact area in more detail, we simulated the behavior of tips with varying degrees of bluntness. The dependence of the simulated *dC/dV* spectra on tip radius of curvature and bluntness angle is shown in Fig. 6(a). The lower portions of the simulated tip geometries are shown in Fig. 6(b). As the tip becomes more blunt the area of tip effectively increases, causing the *dC/dV* peak height to increase as well. The bluntness effect is largest for small tip radius of curvature, as expected based on the preceding discussion of the relative importance of the fringing fields and the increase in depletion depth with increasing contact area. Thus, caution must be exercised in comparison of individual *dC/dV* spectra obtained over periods during which the probe tip geometry might have changed.

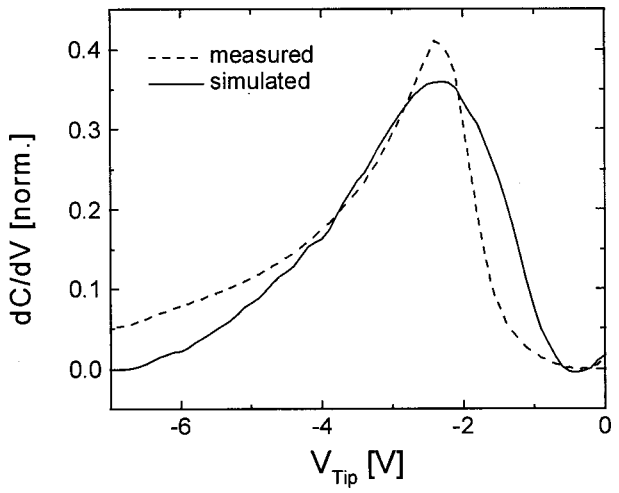

FIG. 8. Comparison of measured *dC/dV* data with simulated *dC/dV* spectrum for a tip with radius of curvature of 30 nm, bluntness angle of 40°, and side angle of 20°. The curves are normalized to the *dC/dV* peak area. The shape of the measured *dC/dV* spectrum is in good agreement with that obtained from the numerical simulations.

We have also assessed the influence of the macroscopic structure of the tip, as quantified by the side angle of the tip, on *dC/dV* spectra shown in Fig. 2. Simulated *dC/dV* spectra for side angles of 15°, 20°, and 25° are shown in Fig. 7. It is apparent from the figure that the side angle has a much smaller influence on the *dC/dV* spectra than the nanoscale tip structure, i.e., the radius of curvature and bluntness.

A comparison of a simulated *dC/dV* spectrum for a tip with a radius of curvature of 30 nm, a bluntness angle of 40°, and a side angle of 20° with the measured *dC/dV* curve from Fig. 1 is shown in Fig. 8. The overall shape of the measured *dC/dV* spectrum is reproduced fairly well for the simulated tip geometry.

The numerical simulations demonstrate that the nanoscale tip structure, characterized by tip radius of curvature and bluntness, influences *dC/dV* spectra strongly, while the macroscopic shape, given by the side angle, has a much smaller influence on the *dC/dV* spectra. This has significant implications for the feasibility of quantitative extraction of parameters such as threshold voltage, layer thickness, and dopant concentrations, and of detailed information about trap states in nitride HFETs and other electronic device structures.

In the case of an $Al_xGa_{1-x}N$/GaN HFET epitaxial layer structure, if the tip radius of curvature and tip bluntness are unknown, it is difficult to extract precise quantitative values for the $Al_xGa_{1-x}N$ thickness or the dopant concentration in the GaN layer from *dC/dV* spectra. A change in $Al_xGa_{1-x}N$ layer thickness would result in a change in accumulation capacitance, while a change in GaN dopant concentration would affect the depletion capacitance. Both parameters would thus change the relative difference between accumulation and depletion capacitance and thus affect the slope in the *C–V* curve and therefore the peak height in the *dC/dV* spectrum. Similar situations can occur in characterization of other electronic device structures, for instance, in dopant profiling of Si structures, where the *dC/dV* peak height varies by approximately a factor of 2 for a tip apex radius of 50 nm over a doping range from 10^{15} to 19^{19} cm^{-3}.[12] Larger changes in peak height can occur if the tip geometry changes. To extract the correct doping, it would be necessary to fit the experimental data with simulated *dC/dV* curves using an accurate description of the tip geometry. If the nanoscale tip structure is not well known, large errors in extracting layer thicknesses or dopant concentrations can occur while fitting experimental data with simulated curves.

Although it is difficult to determine the exact nanoscale tip structure for a given measurement, there are methods to circumvent the above problems. The tip shape might be obtained by deconvolution of topographic images of a sample with a known geometry. In order to obtain information about the nanoscale tip structure, the exact nanoscale structure of the sample must be known. Additional information about the tip shape can be obtained in the following manner. Calibration samples with well-defined and well-characterized layer

thicknesses and dopant concentrations, and a low density of trap states to avoid additional changes in the *dC/dV* spectra, could be used to obtain an approximate tip shape by fitting simulated *dC/dV* spectra for a set of possible tip shapes to *dC/dV* data recorded on the calibration sample. While this method has been demonstrated successfully for Si dopant profiling,[15] it is more difficult to obtain good calibration samples in the $Al_xGa_{1-x}N/GaN$ system due to higher densities of trap states that can affect *dC/dV* spectra significantly. To be able to use this approach, measurements on the calibration sample should be performed before and after the actual experiment to check if the tip shape has changed in the course of the experiment.

The analysis of trap states can be subject to difficulties similar to those described above for extraction of layer thickness and dopant concentration. Trap states can lead to changes in depletion and accumulation capacitance, and in general affect the slope of the *C–V* curve, leading to changes in peak height, width, and position in *dC/dV* spectra. As in the determination of layer thickness and dopant concentration, obtaining quantitative information about trap states by fitting simulated *dC/dV* curves to experimental data is possible, but requires a detailed knowledge of the tip geometry.

IV. CONCLUSIONS

We have presented a detailed analysis of the scanning capacitance spectroscopy technique for measurements of *dC/dV* spectra. The extremely small probe tip size (typical apex radius ~10–30 nm) in SCS measurements makes a detailed analysis incorporating tip–shape effects essential in comparisons of *dC/dV* spectra with standard, large-area *C–V* measurements. Using three-dimensional simulation tools, we have calculated *dC/dV* spectra for various tip geometries by numerically solving Poisson's equation in cylindrical coordinates, with the tip shape parametrized in terms of the radius of curvature, a characteristic bluntness, i.e., the angle up to which the tip remains flat and is in direct contact with the sample, and the side angle. It is found that the nanoscale tip structure, characterized by tip radius of curvature and bluntness, influences *dC/dV* spectra strongly, while the macroscopic shape, given by the side angle, has a much smaller influence on the *dC/dV* spectra. Thus, caution must be exercised in comparison of individual *dC/dV* spectra obtained over periods during which the probe tip geometry might have changed. We have analyzed these effects in detail and assessed their influence on the precise quantitative extraction of parameters such as threshold voltage, doping concentrations, layer thickness, and information about trap states in nitride HFETs and other electronic device structures. Large errors in the extraction of these parameters can occur if the detailed tip geometry is unknown, and simulated curves are fitted to experimental data. To avoid these problems, calibration samples should be used to extract an approximate tip geometry.

ACKNOWLEDGMENTS

The authors thank Dr. H. H. Wieder for useful discussions, and Dr. J. M. Redwing for providing the epitaxial layer structures for this study. Part of this work was supported by NSF Grant No. DMR0072912 and ONR Grant No. N00014-00-1-0135, and POLARIS MURI.

[1] J. J. Kopanski, J. F. Marchiando, and J. R. Lowney, J. Vac. Sci. Technol. B **14**, 242 (1996).
[2] C. C. Williams, W. P. Hough, and S. A. Rishton, Appl. Phys. Lett. **55**, 203 (1989).
[3] C. C. Williams, J. Slinkman, W. P. Hough, and H. K. Wickramasinghe, Appl. Phys. Lett. **55**, 1662 (1989).
[4] K. V. Smith, E. T. Yu, J. M. Redwing, and K. S. Boutros, Appl. Phys. Lett. **75**, 2250 (1999).
[5] D. M. Schaadt, E. J. Miller, E. T. Yu, and J. M. Redwing, Appl. Phys. Lett. **78**, 88 (2001).
[6] J. J. Kopanski, J. F. Marchiando, J. Albers, and B. G. Rennex, AIP Conf. Proc. **449**, 725 (1998).
[7] J. J. McMurray and C. C. Williams, AIP Conf. Proc. **449**, 731 (1998).
[8] J. J. Kopanski, J. F. Marchiando, and J. R. Lowney, Mater. Sci. Eng., B **44**, 46 (1997).
[9] G. Binnig, C. F. Quate, and C. Gerber, Phys. Rev. Lett. **56**, 930 (1986).
[10] Digital Instruments Support Note No. 224, Rev. D (1999).
[11] R. C. Palmer, E. J. Denlinger, and H. Kawamoto, RCA Rev. **43**, 195 (1982).
[12] R. Stephenson, A. Verhulst, P. De Wolf, M. Caymax, and W. Vandervorst, J. Vac. Sci. Technol. B **18**, 405 (2000).
[13] Silvaco International, ATLAS Device Simulator Software (2000).
[14] F. Bernardini, V. Fiorentini, and D. Vanderbilt, Phys. Rev. B **56**, R10024 (1997).
[15] J. J. Kopanski, J. F. Marchiando, and B. G. Rennex, J. Vac. Sci. Technol. B **18**, 409 (2000).